Bulletin of Electrical Engineering and Informatics
Vol. 10, No. 4, August 2021, pp. 1944~1951
ISSN: 2302-9285, DOI: 10.11591/eei.v10i4.3083

Effects of $NaB_2O_4:Mn^{2+}$ and $Ba_2Li_2Si_2O_7:Sn^{3+},Mn^{2+}$ phosphors and remote structure organizations on the white light-emitting diodes with quantum dots and phosphors

Phan Xuan Le, Le Nguyen Hoa Binh
Faculty of Engineering, Van Lang University, Viet Nam

Article Info

Article history:

Received Dec 24, 2020
Revised Apr 28, 2021
Accepted Jun 14, 2021

Keywords:

$Ba_2Li_2Si_2O_7:Sn^{3+},Mn^{2+}$
Bright efficacy
Mie-scattering theory
$NaB_2O_4:Mn^{2+}$
Triple-layer phosphor

ABSTRACT

In order to increase the optical features of white light-emitting diodes (WLEDs), quantum dots (QDs) and phosphor materials have been proposed because of outstanding performance. The configuration of WLEDs with QDs layer and phosphor-silicone layer suggested placing these components separately to limit light loss, and enhance consistency at contact surface of QDs. In this research, the effects of QDs and phosphor on the performance of WLEDs are concluded through experiments. The emitted light and PL spectra were examined thoroughly, and infrared thermal imagers were applied to simulate the heat generation of an actual WLED device. The results show that with the configuration of 60 mA energy source, WLEDs which has the QDs-on-phosphor form attained luminous efficiency (LE) of 110 lm/W, with color rendering index (CRI) of Ra=92 and R9=80, whereas the WLEDs which has the phosphor-on-QDs form only has 68 lm/W in LE, Ra=57 and R9=24. Furthermore, WLEDs which has the QDs-on-phosphor form has less high temperature generated at the components' conjunction in comparison to the counterpart, the peak generated heat in QDs-on-phosphor WLEDs is also lower and the heating capacity gap between 2 structures can go up to 12.3°C.

Corresponding Author:

Phan Xuan Le
Faculty of Engineering
Van Lang University
No. 45 Nguyen Khac Nhu Street, Ho Chi Minh City, Vietnam
Email: le.px@vlu.edu.vn

1. INTRODUCTION

Phosphor converted-light-emitting diodes (pc-LEDs) is a part of solid-state lighting (SSL) and flat screen, which has received much attention in recent time for their ability to achieve high performance quality while having fairly simple fabrication process and low production cost [1]-[3]. The pc-LEDs are mostly created through integration of chromatic radiations from blue LED chip and yellow phosphor $Y_3Al_5O_{12}:Ce^{3+}$ (YAG: Ce). The phosphor material will convert come of the blue light to yellow light, and the combination of blue light and yellow light leads to the emission of white light. This method of pc-LEDs fabrication earns its popularity by performing high luminous efficacy (LE) but is rather poor in color quality due to the lack of chromatic material to improve the color rendering index (CRI) [4]. To advance further with pc-LEDs in lighting industry, researchers have proposed methods adding phosphor material that can compensate for the lack of chromatic light and improve color rendering abilities of pc-LEDs [5]-[8]. However, the spectral emission range of red phosphor is not suitable for white light LEDs and negatively affects the LE [8], [9]. Recently, semiconductor quantum dots (QDs) in SSL applications have attracted numerous researches with their potential to enhance pc-LEDs with strait spectral emission, adjustable bandgap and elevated light

emission rate [10]-[13]. The addition of QDs into pc-LEDs has been proven through experiments to be advantageous to CRI and chromatic performance, and even high light output with the emission wavelength of QDs [14]-[16]. QDs can be merged in pc-LEDs whether through coating a compound of phosphor-silicone gel and QDs onto the chip of the LED or apply remote structure and coat the QDs layer and phosphor layer distinctively [17]-[20]. In the method that blends the components together, QDs is placed into reflection cup and close to the LED chip. The lack of distance between the QDs and the chip (high energy source) causes the deficiency in QDs' stability and lighting output owing to the high thermal generation. The remote type that provides QDs film and the chip a suitable distance, on the other hand, is less affected by the power source, and the discrepancy between the components can be solved through alteration of QDs surrounding environment [21], [22]. This finding suggests that the remote packaging structure should be prioritized in the fabrication process of WLEDs with QDs and phosphor. Thus, the remote structure is proposed in this structure for the QDs-phosphor WLED package. The point is to prevent the heat damage to the QDs while remaining its efficiency. Moreover, we also investigated the two types of remote structure, dual-layer and triple-layer remote structures, to figure out which one is more efficient in terms of WLED optical improvements. The green $Ba_2Li_2Si_2O_7:Sn^{3+},Mn^{2+}$ and red $NaB_2O_4:Mn^{2+}$ phosphors are used to simulate the QDs-remote phosphor structures. The influences of these phosphor on the WLED packages are analyzed to provide a more in-depth understanding on the use of phosphor materials. The objective of this article is to demonstrate the suitable remote phosphor structure for the QDs-WLED package to enhance their efficiency, which helps manufacturers to determine the optimal structure that completely fulfill their goals.

2. METHOD OF RESEARCH

2.1. Preparation of materials from phosphor

To conduct the experiment, we must first obtain the phosphor material which will be presented in this section. The green $Ba_2Li_2Si_2O_7:Sn^{3+},Mn^{2+}$ phosphor is created through 4 steps: mixing, and 3 consecutive firing processes. The $BaCO_3$, SiO_2 and Li_2CO_3 ingredients of the green phosphor are blended to create a compound through milling or dry grinding. Put the mixture of ingredients from previous step in open boats and fire with H_2 at 850°C for an hour. Then add in the remaining ingredients SnO, $MnCO_3$, NH_4Br, and methanol, begin to stir the compound until it is mixed well. After that, leave the compound to dry and grind into powder [23], [24]. The powder will then be placed in capped quartz tube and fired with N_2 at 850°C for an hour. Repeat to grind the product from previous step to powder and procced with the final firing process in uncovered quartz boats with CO at 850°C for 16 hours. Grind the compound into powder and store in container with seal to avoid contamination. The resulted green phosphor will have green color emission and emission peak of 2.32 eV. Table 1 demonstrates the chemical composition for the $Ba_2Li_2Si_2O_7:Sn^{3+},Mn^{2+}$ phosphor. The fabrication of red phosphor $NaB_2O_4:Mn^{2+}$ is introduced with 3 steps. First, the compound of ingredient is formed through grinding or milling. Then fire the compound in uncovered quartz boat with N_2 at 500°C and then powderize the product. Begin to another firing process in uncovered quartz boat with N_2 at 700°C for an hour and then grind the result into powder. Next, prepare for a firing process in open quartz boat with N_2, however, the firing period and temperature are decided by the type of structure with α structure is fired at 1000°C for 2 hours and β structure is fired at 850°C for 4 hours. The completed red $NaB_2O_4:Mn^{2+}$ phosphor will have red color light emission and 1.88 eV or 2.11 emission peaks. The chemical composition of $NaB_2O_4:Mn^{2+}$ is shown in Table 2.

Table 1. Chemical composition of green phosphor $Ba_2Li_2Si_2O_7:Sn^{3+},Mn^{2+}$

Ingredient	Mole %	By weight (g)
$BaCO_3$	93.5	185
SiO_2	110 (of Li)	41
Li_2CO_3	110	66
SnO	5	6.8
$MnCO_3$	1.5	1.7
NH_4Br	50	49

Table 2. Chemical composition of red phosphor $NaB_2O_4:Mn^{2+}$

Ingredient	Mole %	By weight (g)
MgO	98	40
$MnCO_3$	2	2.3
H_3BO_3	205	127

2.2. Simulation process

The polymer matrix is an important part of the research and in this case, we chose the polymethyl methacrylate (PMMA) for the QDs film. The preparation process of QDs-PMMA film is supported by the situ polymerization method. The ingredients of MMA monomer 10 ml and azodiisobutyronitrile (AIBN, 0.2% wt/wt as for MMA) 25 ml are put into a three-neck flask and being stirred to dissolve the AIBN entirely. Later, 20 mg of CdSe/ZnS QDs as-prepared solvated in toluene added to the flask through small drops and then blend is distributed evenly using ultrasound treatment. In the next step, place the flask into the 70°C thermostatic water bath for 15 min until the blend start to become denser, and then proceed to cool the mixture. The mixture will be placed into a mold and being vacuumed for 24 hours in the oven at 45°C. The final result was divided into squares in order to be applied for the module of LED. The phosphor-silicone membrane is processed with an ordinary heat treating method. At first 0.3 g of YAG phosphor with maximum emission wavelength of 550 nm (bought from Intermatix) and 1 g of silicone gel (OE 6550, bought from Dow Corning) was 20-min merged and stirred before distribution. The alternating cycles of vacuum were applied during the stirring process to remove the bubbles. After the steps above, the mixture will be put in designed mold and vacuumed in oven at 150°C for 1 hour. The final product is also modified into squares. The WLEDs device is created by pouring clean silicone gel into the interior gap of 2835 SMD LED, and then placing the QDs layer and/or phosphor membrane into the structure and treating the configuration with heat at 120°C for 30 minutes.

Each layer of phosphor is fixed at 0.08 mm thickness. Besides, the YAG:Ce^{3+} in the configuration is also an essential detail, therefore, it must be changed accordingly to the fluctuation of concentration of green or red phosphor to uphold the average correlated color temperatures (ACCTs). Additionally, at each varied ACCT of structure of phosphor, the YAG:Ce^{3+} concentrations are various, which makes the variety of scattering specificity within WLEDs. Moreover, this discrepancy leads to the differences in optical properties, see Figure 1.

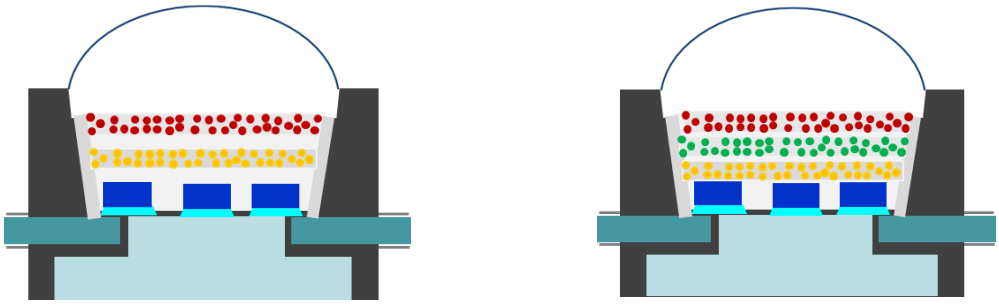

(a) (b)

Figure 1. Illustration of white LEDs multi-layer phosphor structures, (a) dual-layer phosphor (DL), (b) triple-layer phosphor (TL)

From Figure 2 and Figure 3, the amount of yellow phosphor YAG:Ce^{3+} of DL structure is higher than TL structure regardless of ACCTs. The high amount of YAG:Ce^{3+}in the package will cause more light loss due to back-scattered and lower the luminous flux at all color temperatures. In addition, excessive YAG:Ce^{3+} leads to low quality of emitted light because the chromatic light components of yellow, red, and green are not balanced. The proposed solution for back-scattering is to increase the red component which is available in red phosphor. On the other hand, green phosphor is effective in terms of chromatic uniformity and light output enhancement. The triple-layer distant phosphor with three distinct phosphor layers of red, yellow, and blue seems to be the appropriate structure regarding the its effects on optical performance of WLEDs. However, the performance of TL structure must be considered through practical scenario before concluding, thus, the following section will demonstrate experiments conducted to provide references for TL structure efficiency.

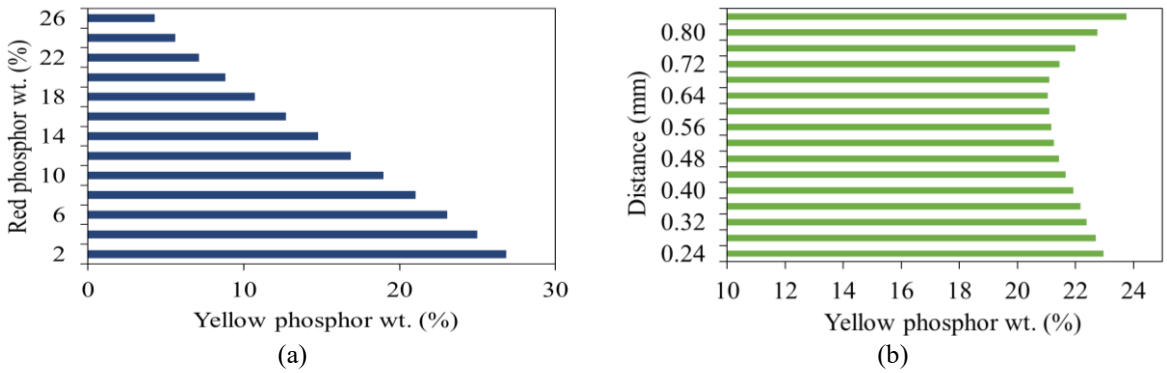

Figure 2. The concentration of yellow YAG:Ce^{3+} phosphor in each distant phosphor structure at each dissimilar ACCT, (a) DL, (b) TL

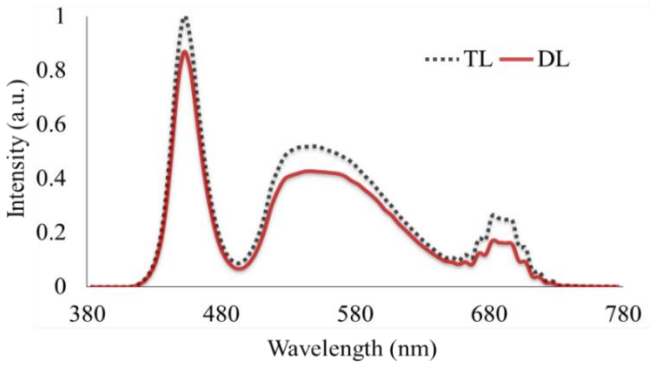

Figure 3. Emission spectra of phosphor configurations

3. RESULTS AND ANALYSIS

Figure 4 illustrates that CRI in dual-layer (DL) is higher than triple-layer (TL) when both structures are in remote phosphor configurations. The higher CRI at all ACCT of DL proves that DL is optimal for CRI and is still effective in WLEDs at 8500 K. With this result, the manufactures can easily improve CRI for remote phosphor structures, especially, for devices over 7000 K, which is still considered challenging. The advantage in CRI is contributed by red $NaB_2O_4:Mn^{2+}$ phosphor layer. The TL structure is not as effective as DL in terms of CRI, therefore, in mass production of WLEDs with high CRI, the DL structure is the more efficient choice. However, CRI in comparison with CQS does not have the same value. CQS which combines three factors: CRI, choices of viewers, and chromaticity coordinate, is more reliable and thorough quality indicator for WLEDs. Many researchers have been using CQS in their research and even prioritize this scale when evaluating the chromaticity of WLEDs. In this study, we studied the CQS and presented them in Figure 5 for reference. From the results, TL with three colors red, yellow and green is able to control the color quality far better than DL and therefore achieves higher CQS.

Figure 5 suggests that WLEDs with high color quality should be created with TL structure because TL has higher CQS and higher CQS means better chromatic performance. However, most WLEDs with higher color quality will suffer some light output damage. To investigate this theory on TL light output, we compare the emitted luminous flux between the dual-layer and triple-layer structures, see Figure 6. In this part, the mathematical model of the passed through blue light and transformed yellow light in the triple-layer phosphor form are demonstrated in details to discuss the improvement that can be yielded from these parts. The passed through blue light and transformed yellow light for double-layer remote package with the phosphor layer thickness of h are expressed as [25], [26]:

$$PB_2 = PB_0 e^{-\alpha_{B_2} h} e^{-\alpha_{B_2} h} = PB_0 e^{-2\alpha_{B_2} h} \quad (1)$$

$$\begin{aligned} PY_2 &= \frac{1}{2}\frac{\beta_2 PB_0}{\alpha_{B_2}-\alpha_{Y_2}}\left[e^{-\alpha_{Y_2} h} - e^{-\alpha_{B_2} h}\right] e^{-\alpha_{Y_2} h} + \frac{1}{2}\frac{\beta_2 PB_0}{\alpha_{B_2}-\alpha_{Y_2}}\left[e^{-\alpha_{Y_2} h} - e^{-\alpha_{B_2} h}\right] \\ &= \frac{1}{2}\frac{\beta_2 PB_0}{\alpha_{B_2}-\alpha_{Y_2}}\left[e^{-2\alpha_{Y_1} h} - e^{-2\alpha_{B_1} h}\right] \end{aligned} \quad (2)$$

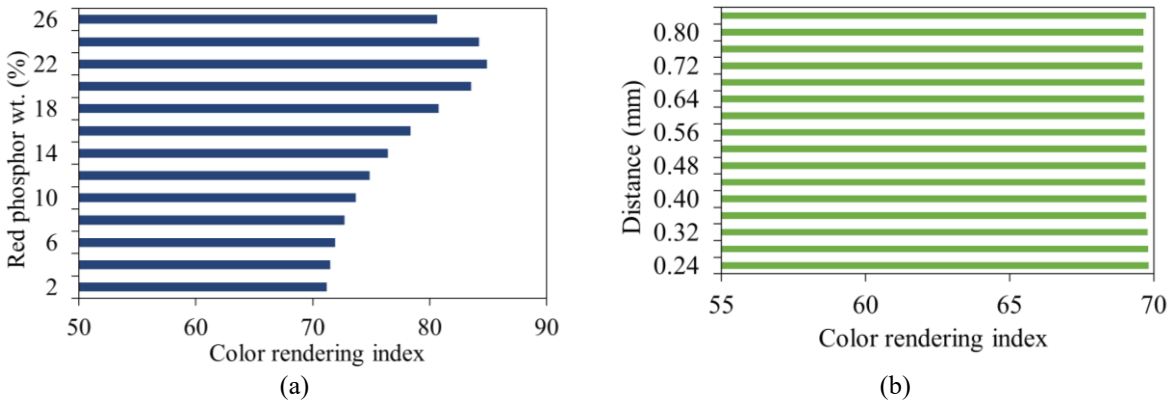

Figure 4. Color rendering index of phosphor configurations in accordance with ACCTs, (a) DL, (b) TL

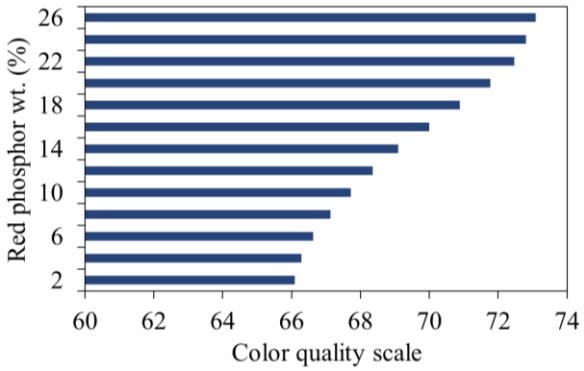

Figure 5. Color quality scale of phosphor configurations in accordance with ACCTs

The passed through blue light and transformed yellow light for three-layer remote package with the phosphor layer thickness of $\frac{2}{3}$ are determined in following expressions:

$$PB_3 = PB_0.e^{-\alpha_{B_2}\frac{2h}{3}}.e^{-\alpha_{B_2}\frac{2h}{3}}.e^{-\alpha_{B_2}\frac{2h}{3}} = PB_0.e^{-2\alpha_{B_3}h} \tag{3}$$

$$\begin{aligned} PY'_3 &= \frac{1}{2}\frac{\beta_3 PB_0}{\alpha_{B_3}-\alpha_{Y_3}}\left[e^{-\alpha_{Y_3}\frac{2h}{3}} - e^{-\alpha_{B_3}\frac{2h}{3}}\right]e^{-\alpha_{Y_3}\frac{2h}{3}} + \frac{1}{2}\frac{\beta_3 PB_0 e^{-\alpha_{B_3}\frac{2h}{3}}}{\alpha_{B_3}-\alpha_{Y_3}} \\ &\quad \left[e^{-\alpha_{Y_3}\frac{2h}{3}} - e^{-\alpha_{B_3}\frac{2h}{3}}\right] \\ &= \frac{1}{2}\frac{\beta_3 PB_0}{\alpha_{B_3}-\alpha_{Y_3}}\left[e^{-\alpha_{Y_3}\frac{4h}{3}} - e^{-2\alpha_{B_3}\frac{4h}{3}}\right] \end{aligned} \tag{4}$$

$$\begin{aligned} PY_3 &= PY'_3.e^{-\alpha_{Y_3}\frac{2h}{3}} + PB_0.e^{-2\alpha_{B_3}\frac{4h}{3}}\frac{1}{2}\frac{\beta_3}{\alpha_{B_3}-\alpha_{Y_3}}\left[e^{-\alpha_{Y_3}\frac{2h}{3}} - e^{-\alpha_{B_3}\frac{2h}{3}}\right] \\ &= \frac{1}{2}\frac{\beta_3 PB_0}{\alpha_{B_3}-\alpha_{Y_3}}\left[e^{-\alpha_{Y_3}\frac{4h}{3}} - e^{-\alpha_{B_3}\frac{4h}{3}}\right]e^{-\alpha_{Y_3}\frac{2h}{3}} + \frac{1}{2}\frac{\beta_3 PB_0 e^{-\alpha_{B_3}\frac{4h}{3}}}{\alpha_{B_3}-\alpha_{Y_3}} \\ &\quad \left[e^{-\alpha_{Y_3}\frac{2h}{3}} - e^{-\alpha_{B_3}\frac{2h}{3}}\right] \\ &= \frac{1}{2}\frac{\beta_3 PB_0}{\alpha_{B_3}-\alpha_{Y_3}}\left[e^{-\alpha_{Y_3}h} - e^{-2\alpha_{B_3}h}\right] \end{aligned} \tag{5}$$

In these expressions above, the thickness of each phosphor layer is called h. The subscripts as "2" and "3" are used to depict double-layer and triple-layer distant phosphor structures, respectively. β indicates the conversion coefficient for blue light transforming to yellow light. γ is the reflection coefficient of the yellow light. The light intensity from blue LED which includes the intensities of blue light (PB) and yellow

light (*PY*), presented by PB_0. α_B; α_Y are parameters depicting the fractions of the energy loss of blue and yellow lights during their spread in the phosphor layer in turn. In addition, PY'_3 in expression (4) describes the yellow transmitted light going through two layers of phosphor. With the triple-layer phosphor form, the lighting efficiency of pc-LEDs is promoted greatly in comparison with a dual-layer one:

$$\frac{(PB_3-PY_3)-(PB_2+PY_2)}{(PB_2+PY_2)} > \frac{e^{-2\alpha_{B_3}h}-e^{-2\alpha_{B_2}h}}{e^{-2\alpha_{Y_3}h}-e^{-2\alpha_{B_2}h}} > 0 \quad (6)$$

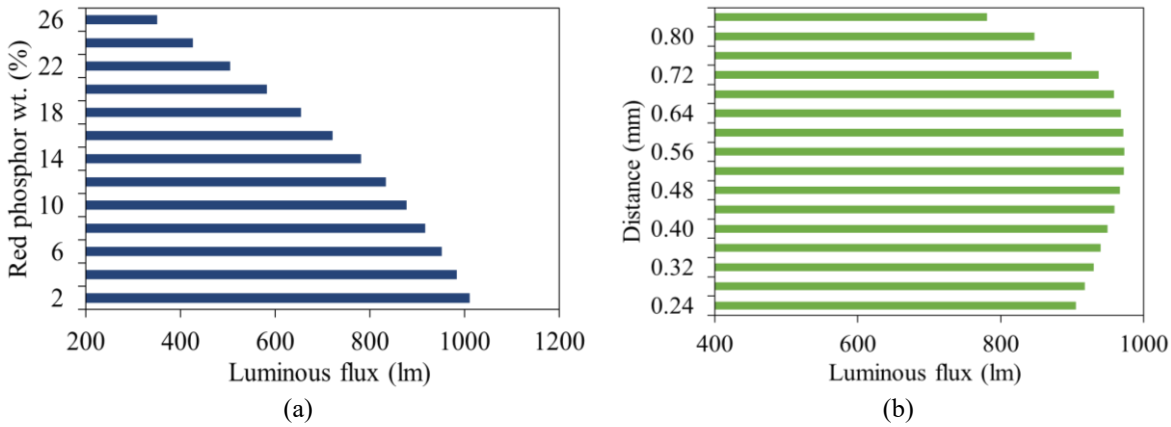

Figure 6. Luminous output (LO) of phosphor configurations in accordance with ACCTs, (a) DL, (b) TL

The angular dependency of each component was demonstrated means the relation between the component position and emission spectrum exist. The large-wavelength in the spectra are uniformly distributed, while at lower wavelengths the performance will vary depends on the angle. Moreover, the alternating distribution model of the green part and the sudden variation in the distribution of the blue counterpart can be explained by different reasons. Some of the reasons are the particles scattering of the component wavelengths, comparative transparency of the segmented plates, and the organization of the materials plates. The similarities in the amount and position of the green $Ba_2Li_2Si_2O_7:Sn^{3+},Mn^{2+}$ and red $NaB_2O_4:Mn^{2+}$ phosphors proven that the theory is true. In addition, the higher light scattering at high angles verified that phosphor-to-glass ratio applied in each material plate impacts the intensity distribution of the colors in the configuration. The results suggest that the angular dependence from previous section can be optimized by modifying the process of the PiG. In particular, the blue light relative intensity would be estimated, instead of managing the chromatic discharge by changing the proportion of the green to red phosphors in the correlative components. The green $Ba_2Li_2Si_2O_7:Sn^{3+},Mn^{2+}$ has more phosphor particles than the other phosphor gives bright green emission and decreases the transparency of the blue part of the spectrum. This assumption is proven by the evidence from the fairly intensity distribution of the component colors from different angles. Low phosphor concentration in green part of the PiG is the cause for angular dependence reduction of the blue light because it allows more blue emitted light to escape than higher phosphor concentrations. The angular reliance of both the green and blue components is impacted by the actual amount of light escape the configuration. In addition, because blue light are mostly converted by green phosphor layer therefore, was not received much attention. Nevertheless, the highest intensity of the blue part appears when there are red components from the chromatic plate. This comes from the 1:2 proportion between red and green phosphor that makes large amount of the emitted blue light to be transmitted through the red part. Accordingly, the high-intensity area of the green and blue occurs in alternating quadrants of the polar diagram.

These outcomes show that the distant configuration can be used for spectral properties adjustment, which is the reason why remote WLEDs is replacing conventional LED packaging in modern lighting. This means CIE can be enhanced through correct structure and method of fabrication in addition to other factors such as particles sizes and layer thickness. The angular dependence of light output exists mostly because of PiG material traits. In addition, the design and fabrication that separate and create layers of the PiG will leads to more innovative LED design; the changeable optical characteristics will also be achievable. The 4-segmented PiG currently being used can potentially be divided into eight even segments to place at 45° of the center of a colored segment angle with distinct color. This luminescence can be further improved through

angular dependence reduced from this structure. Furthermore, in case the radiation from blue LED chips creates an angular-dependent light instead of homogeneously distributed light, then the comparative angular wideness of the components with tunable chromaticity can alter, see Figure 7.

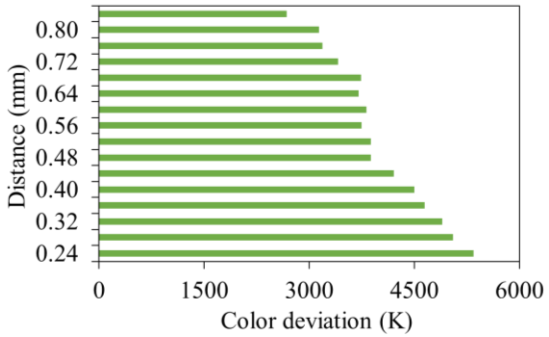

Figure 7. Correlated color temperature deviation (D-CCT) of distant phosphor configurations in accordance with ACCTs

4. CONCLUSION

In this study, we proposed theory and conducted experiments to evaluate the performances of multi-layer remote WLEDs, one with two phosphor layers and the other with three layers. The total lighting capacity and PL spectra were examined with the calculation results achieved from integrating sphere formation. The degree of hotness fields was replicated by putting the optical measurements into heat imitation, and eventually validated by infrared thermal imager. From the experiments results calculated with power source of 60 mA, the WLED has the QDs-on-phosphor form WLEDs attained 110 lm/W in LE, and Ra=92, R9=80 in color rendering index (CRI), whereas the WLEDs which has the phosphor-on-QDs form achieved 68 lm/W LE, Ra=57, and R9=24. Furthermore, WLEDs which has the QDs-on-phosphor form has better thermal performance than the other structure even highest heat generated from the QDs-on-phosphor is lower with the highest discrepancy of 12.3°C. Therefore, when choosing device configuration, the QDs-on-phosphor is apparently the better option considering the optical efficiency, color quality and consistency as well as thermal performance.

REFERENCES

[1] Sadra Sadeghi, Baskaran Ganesh Kumar, Rustamzhon Melikov, Mohammad Mohammadi Aria, Houman Bahmani Jalali, Sedat Nizamoglu, "Quantum dot white LEDs with high luminous efficiency," *Optica*, vol. 5, no. 7, pp. 793-802, 2018, doi: 10.1364/OPTICA.5.000793.

[2] S. Pan, B. Yang, X. Xie, Z. Yun, "Image restoration and color fusion of digital microscopes," *Applied Optics*, vol. 58, no. 9, pp. 2183-2189, 2019, doi: 10.1364/AO.58.002183.

[3] O. Kunieda and K. Matsushima, "High-quality full-parallax full-color three-dimensional image reconstructed by stacking large-scale computer-generated volume holograms," *Appl. Opt.*, vol. 58, no. 34, pp. G104-G111, 2019, doi: 10.1364/AO.58.00G104.

[4] Hussein S. El-Ghoroury, Yoshitake Nakajima, Milton Yeh, Evan Liang, Chih-Li Chuang, and J. C. Chen, "Color temperature tunable white light based on monolithic color-tunable light emitting diodes," *Optics Express*, vol. 28, no. 2, pp. 1206-1215, 2020, doi: 10.1364/OE.375320.

[5] Q. Song, *et al.*, "Vicarious calibration of COCTS-HY1C at visible and near-infrared bands for ocean color application," *Optics Express*, vol. 27, no. 20, pp. A1615-A1626, 2019, doi: 10.1364/OE.27.0A1615.

[6] Pedro J. Pardo, María Isabel Suero, Ángel Luis Pérez, "Correlation between perception of color, shadows, and surface textures and the realism of a scene in virtual reality," *Journal Optical Society of America*, vol. 35, pp. B130-B135, 2018, doi: 10.1364/JOSAA.35.00B130.

[7] Y. L. Piao, M. U. Erdenebat, K. C. Kwon, S. K. Gil, N. Kim, "Chromatic-dispersion-corrected full-color holographic display using directional-view image scaling method," *Applied Optics*, vol. 58, no. 5, pp. A120-A127, 2019, doi: 10.1364/AO.58.00A120.

[8] K. Matsushima and N. Sonobe, "Full-color digitized holography for large-scale holographic 3D imaging of physical and nonphysical objects," *Applied Optics*, vol. 57, no. 1, pp. A150-A156, 2018, doi: 10.1364/AO.57.00A150.

[9] Y. Z. Jiang, *et al.*, "Luminescence of Tb^{3+}/Eu^{3+} codoped LiYF4 single crystals under UV excitation for white-light LEDs," *Chinese Optics Letters*, vol. 13, no. 7, pp. 071601, 2015, doi: 10.3788/COL201513.071601.

[10] F. Guan, G. Jiang, Y. Song, M. Yu, Z. Peng, F. Chen, "No-reference high-dynamic-range image quality assessment based on tensor decomposition and manifold learning," *Applied Optics*, vol. 57, no. 4, pp. 839-848, 2018, doi: 10.1364/AO.57.000839.
[11] J. J. Gómez-Valverde, *et al.*, "Automatic glaucoma classification using color fundus images based on convolutional neural networks and transfer learning," *Biomedical Optics Express*, vol. 10, no. 2, pp. 892-913, 2019, doi: 10.1364/BOE.10.000892.
[12] Q. Zaman, *et al.*, "Two-color surface plasmon resonance nanosizer for gold nanoparticles," *Optics Express*, vol. 27, no. 3, pp. 3200-3216, 2019, doi: 10.1364/OE.27.003200.
[13] D. Durmus and W. Davis, "Blur perception and visual clarity in light projection systems," *Optics Express*, vol. 27, no. 4, pp. A216-A223, 2019, doi: 10.1364/OE.27.00A216.
[14] Ryuji Hirayama, Hirotaka Nakayama, Atushi Shiraki, Takashi Kakue, Tomoyoshi Shimobaba, and Tomoyoshi Ito, "Projection of multiple directional images on a volume structure with refractive surfaces," *Optics Express*, vol. 27, no. 20, pp. 27637-27648, 2019, doi: 10.1364/OE.27.027637.
[15] Christoph Polzer, *et al.*, "Correlative two-color two-photon (2C2P) excitation STED microscopy," *Biomedical Optics Express*, vol. 10, no. 9, pp. 4516-4530, 2019, doi: 10.1364/BOE.10.004516.
[16] Fabian Bergermann, Lucas Alber, Steffen J. Sahl, Johann Engelhardt, and Stefan W. Hell, "2000-fold parallelized dual-color STED fluorescence nanoscopy," *Optics Express*, vol. 23, no. 1, pp. 211-223, 2015, doi: 10.1364/OE.23.000211.
[17] Benjamin K. Tsai, Catherine C. Cooksey, David W. Allen, Christopher C. White, Eric Byrd, and Deborah Jacobs, "Exposure study on UV-induced degradation of PTFE and ceramic optical diffusers," *Applied Optics*, vol. 58, no. 5, pp. 1215-1222, 2019, doi: 10.1364/AO.58.001215.
[18] V Fuertes, J. F. Fernández, and E. Enríquez, "Enhanced luminescence in rare-earth-free fast-sintering glass-ceramic," *Optica*, vol. 6, no. 5, pp. 668-679, 2019, doi: 10.1364/OPTICA.6.000668.
[19] H. Kim, Y. J. Seo, and Y. Kwak, "Transparent effect on the gray scale perception of a transparent OLED display," *Optics Express*, vol. 26, no. 4, pp. 4075-4084, 2018, doi: 10.1364/OE.26.004075.
[20] Jana Zujovic, Thrasyvoulos N. Pappas, David L. Neuhoff, René van Egmond, and Huib de Ridder," Effective and efficient subjective testing of texture similarity metrics," *Journal of the Optical Society of America A*, vol. 32, no. 2, pp. 329-342, 2015, doi: 10.1364/JOSAA.32.000329.
[21] B. Zhang, *et al.*, "Rapid, large-scale stimulated Raman histology with strip mosaicing and dual-phase detection," *Biomedical Optics Express*, vol. 9, no. 6, pp. 2604-2613, 2018, doi: 10.1364/BOE.9.002604.
[22] Marites M. Magno-Canto, Lachlan I. W. McKinna, Barbara J. Robson, and Katharina E. Fabricius," Model for deriving benthic irradiance in the Great Barrier Reef from MODIS satellite imagery," *Optics Express*, vol. 27, no. 20, pp. A1350-A1371, 2019, doi: 10.1364/OE.27.0A1350.
[23] W. Gao, K, Ding, G, He, P. Zhong, "Color temperature tunable phosphor-coated white LEDs with excellent photometric and colorimetric performances," *Applied Optics*, vol. 57, no. 31, pp. 9322-9327, 2018, doi: 10.1364/AO.57.009322.
[24] H. L. Ke, *et al.*, "Lumen degradation analysis of LED lamps based on the subsystem isolation method," *Applied Optics*, vol. 57, no. 4, pp. 849-854, 2018, doi: 10.1364/AO.57.000849.
[25] S. Beldi, *et al.*, "High Q-factor near infrared and visible Al2O3-based parallel-plate capacitor kinetic inductance detectors," *Optics Express*, vol. 27, no. 9, pp. 13319-13328, 2019, doi: 10.1364/OE.27.013319.
[26] Y. Chu, *et al.*, "Perception enhancement using importance-driven hybrid rendering for augmented reality based endoscopic surgical navigation," *Biomedical Optics Express*, vol. 9, no. 11, pp. 5205-5226, 2018 doi: 10.1364/BOE.9.005205.